Chinese Chemical Letters 36 (2025) 110146

Contents lists available at ScienceDirect

Chinese Chemical Letters

journal homepage: www.elsevier.com/locate/cclet

Glycoengineering-assistant biomineralization for tumor blockade therapy

Yang Liu [a,b], Minglu Li [a,*], Jianxun Ding [a,b,c,*], Xuesi Chen [a,b,c]

[a] Key Laboratory of Polymer Ecomaterials, Changchun Institute of Applied Chemistry, Chinese Academy of Sciences, Changchun 130022, China
[b] School of Applied Chemistry and Engineering, University of Science and Technology of China, Hefei 230026, China
[c] Jilin Biomedical Polymers Engineering Laboratory, Changchun Institute of Applied Chemistry, Chinese Academy of Sciences, Changchun 130022, China

ARTICLE INFO

Article history:
Received 10 May 2024
Revised 18 June 2024
Accepted 20 June 2024
Available online 21 June 2024

Keywords:
Metabolic glycoengineering
Click chemistry
Bioorthogonal reaction
Biomineralization
Tumor blockade therapy

ABSTRACT

Tumor blockade therapy inhibits tumor progression by cutting off essential supplies of nutrients, oxygen, and biomolecules from the surrounding microenvironments. Inspired by natural processes, tumor biomineralization has evolved due to its biocompatibility, self-reinforcing capability, and penetration-independent mechanism. However, the selective induction of tumor biomineralization using synthetic tools presents a significant challenge. Herein, a metabolic glycoengineering-assistant tumor biomineralization strategy was developed. Specifically, the azido group (N_3) was introduced onto the cytomembrane by incubating tumor cells with glycose analog Ac_4ManNAz. In addition, a bisphosphonate-containing polymer, dibenzocyclooctyne-poly(ethylene glycol)-alendronate (DBCO-PEG-ALN, DBPA) was synthesized, which attached to the tumor cell surface *via* "click chemistry" reaction between DBCO and N_3. Subsequently, the bisphosphonate group on the cell surface chelated with positively charged ions in the microenvironments, triggering a consecutive process of biomineralization. This physical barrier significantly reduced tumor cell viability and mobility in a calcium ion concentration-dependent manner, suggesting its potential as an effective anti-tumor strategy for *in vivo* applications.

Tumor blockade therapy represents a promising strategy for tumor suppression, which hampers the normal physiological functions of malignant cells by disrupting the communication between the tumor and its surrounding microenvironments [1]. Rather than eliminating unwanted cells directly, it obstructs the essential supplies of nutrients, oxygen, and biomolecules, leading to reduced cell motility and decreased viability [2,3]. Generally, tumor blockade therapy involves vessel blockade [4-6], the introduction of artificial extracellular matrix [7,8], and biomineralization [9]. Among these, biomineralization is particularly noteworthy due to its biocompatibility and self-reinforcing capability using endogenous substances [10]. Notably, chemical tools that trigger biomineralization function at the peripheral area of tumor tissue. Thus, there is no need to navigate the high interstitial fluid pressure typically found within the tumor microenvironments or to cross endosomal barriers to reach the intracellular compartment, which circumvents the limitations that compromise the efficacy of many cell-targeting chemotherapeutics [11-13].

In our previous studies, we initiated biomineralization around the tumor tissue by preparing bisphosphonate-containing polymers, including 1,2-distearoyl-*sn*–glycero-3-phosphoethanolamine-*N*-poly(ethylene glycol)-alendronate (DPA) and dodecylamine-poly((γ-dodecyl-L-glutamate)-*co*-(L-histidine))-*block*-poly(L-glutamate-*graft*-alendronate) (BINP) [3,14,15]. It was proved that the biomineralized barrier around osteosarcoma indeed contributed to tumor growth suppression, pulmonary metastasis elimination, and bone erosion remission. Compared with DPA that was inserted into the cytomembrane without selectivity, the addition of a histidine component to the polypeptide-based BINP allowed it to respond to the mildly acidic microenvironments, endowing it with a tumor-selective property [16,17]. Specifically, tumor cells incubated with BINP at pH 6.5 had a calcium content 1.35 times higher after 12 h incubation than those incubated at pH 7.4. However, realizing specific tumor cell biomineralization remains a significant challenge.

Bioorthogonal "click chemistry" encompasses a suite of reactions that proceed under physiological conditions without interfering with inherent biochemical processes [18,19]. Among these, the reaction between the dibenzocyclooctyne (DBCO) and azido group (N_3) is noted for its efficiency, selectivity, and catalyst-free properties [20]. Leveraging this principle, a metabolic glycoengineering

* Corresponding authors.
E-mail addresses: mlli123@ciac.ac.cn (M. Li), jxding@ciac.ac.cn (J. Ding).

https://doi.org/10.1016/j.cclet.2024.110146
1001-8417/

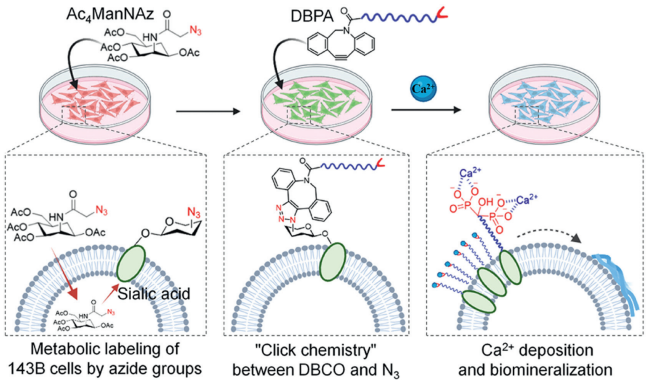

Scheme 1. Glycoengineering-assistant tumor cell biomineralization.

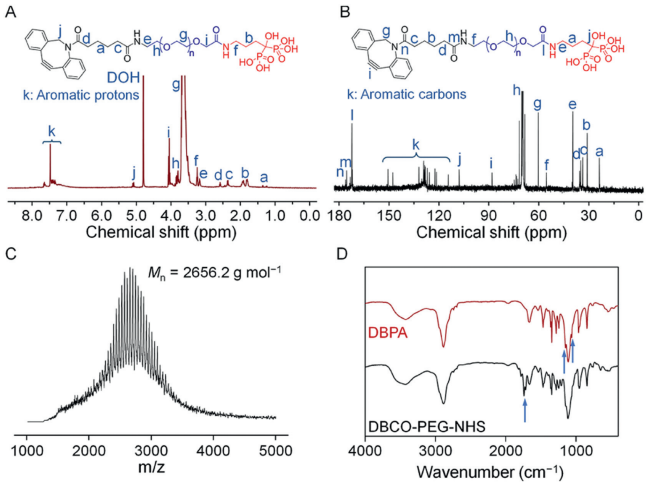

Fig. 1. Chemical characterizations of DBPA. (A) ^{1}H NMR and (B) ^{13}C NMR spectra of DBPA in D_2O. (C) MALDI-TOF MS spectrum of DBPA. (D) FT-IR spectra of DBPA and DBCO-PEG-NHS. Blue arrows represent alterations of characteristic absorption peaks.

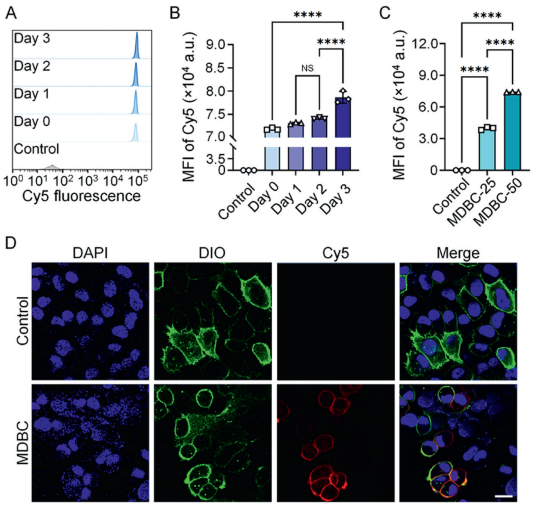

Fig. 2. Metabolic glycan labeling of 143B cells with N_3. (A) Representative Cy5 histograms and (B) quantified MFI of 143B cells incubated without or with 50.0 μmol/L Ac_4ManNAz for 1, 2, or 3 days and then stained with DBCO-Cy5. 143B cells treated with PBS were used as the Control group. (C) MFI of 143B cells incubated with 25.0 or 50.0 μmol/L of Ac_4ManNAz for 3 days and then stained with DBCO-Cy5. (D) CLSM images of Ac_4ManNAz-pretreated 143B cells that were then incubated with DBCO-Cy5. Cell nuclei and membranes were stained with 4′,6-diamidino-2-phenylindole (DAPI) and 3,3′-dioctadecyloxacarbocyanine perchlorate (DIO), respectively. Scale bar: 20 μm. Statistical data are represented as mean ± SD ($n = 3$). NS: not significant. $^{****}P < 0.0001$. Student's *t*-test.

strategy was adopted to facilitate targeted tumor cell biomineralization [21,22]. We designed a biomineralization-initiating polymer, dibenzocyclooctyne-poly(ethylene glycol)-alendronate (DBCO-PEG-ALN, DBPA), which consists of three functional components: DBCO group to mediate "click chemistry" reaction, the hydrophilic segment PEG, and the biomineralization-inducing component ALN. As depicted in Scheme 1, N_3 was tagged onto the targeted cells through the metabolism of mannose derivate Ac_4ManNAz for sialic acid biosynthesis. DBPA was then anchored efficiently to the cell membrane *via* a "click chemistry" reaction between DBCO and N_3. Subsequently, bisphosphonate groups attracted calcium ions (Ca^{2+}) from the microenvironments, initiating biomineralization around tumor cells. This glycoengineering-assistant biomineralization ensures the selective blockade of cells marked with N_3, enhancing both the biosafety and therapeutic efficacy of blockade therapy.

DBPA was readily synthesized by reacting the *N*-hydroxysuccinimide (NHS) group of DBCO-PEG-NHS and the amine group of alendronate sodium (Scheme S1 in Supporting information). The successful attachment of ALN onto DBPA was confirmed by proton nuclear magnetic resonance (^{1}H NMR) and carbon nuclear magnetic resonance (^{13}C NMR) spectra (Figs. 1A and B). Compared with the ^{1}H NMR spectrum of DBCO-PEG-NHS in Fig. S1 (Supporting information), the emergence of new characteristic peaks—peak b ($-CH_2CH_2CH_2-$, 1.80, 1.90 ppm) and peak f ($-NHCH_2CH_2-$, 3.24 ppm)—in the ^{1}H NMR spectrum of DBPA demonstrated the successful grafting of ALN. The integration area of peak b indicated that the substitution ratio of NHS groups by ALN was about 95.8%. Additionally, the matrix-assisted laser desorption/ionization time-of-flight mass spectrometry (MALDI-TOF MS) spectrum revealed that the molecular weight of DBPA was about 2600 Da (Fig. 1C). The disappearance of the peak corresponding to stretching vibration $\nu_{C=O}$ at 1710–1750 cm^{-1} in the Fourier transform-infrared (FT-IR) spectrum for DBPA compared with the spectrum of DBCO-PEG-NHS illustrated the complete substitution of NHS groups (Fig. 1D). Peaks at 1150 and 1060 cm^{-1} could be ascribed to the stretching vibrations of ν_{P-O} and ν_{C-O} in the ALN component, respectively, proving the successful grafting of ALN onto DBPA.

Following the successful synthesis of DBPA, we sought to determine the optimal conditions for labeling 143B cell membrane with N_3. To this end, 143B cells were incubated in media supplemented with 50.0 μmol/L Ac_4ManNAz for 1, 2, or 3 days, respectively. After each period, the cells were exposed to DBCO cyanine5 (DBCO-Cy5) for 30 min. A control group of tumor cells, cultured with DBCO-Cy5 but without Ac_4ManNAz pretreatment, was also established for comparison. As indicated in Figs. 2A and B, the mean fluorescence intensity (MFI) of tumor cells showed no apparent differences between groups pretreated with Ac_4ManNAz for 1 or 2 days, whereas 3-day incubation significantly increased the amount of N_3 attached. Specifically, the MFI of 143B cells pretreated with Ac_4ManNAz for 3 days increased by 9.4% compared with those treated with DBCO-Cy5 only, confirming the successful "click chemistry" reaction between DBCO and N_3. Furthermore, as shown in Fig. 2C, the MFI was more remarkable in cells treated with 50.0 μmol/L than those treated with 25.0 μmol/L Ac_4ManNAz. Based on these findings, an Ac_4ManNAz concentration of 50.0 μmol/L and a 3-day metabolic labeling period were used for subsequent experiments. To visually confirm the successful labeling, 143B cells were examined using confocal laser scanning microscopy (CLSM). The microscopy results, depicted in Fig. 2D, showed bright red fluorescence of DBCO-Cy5 co-localizing with the green fluorescence of cytomembrane marker, demonstrating the existence of N_3 on the tumor cell surface.

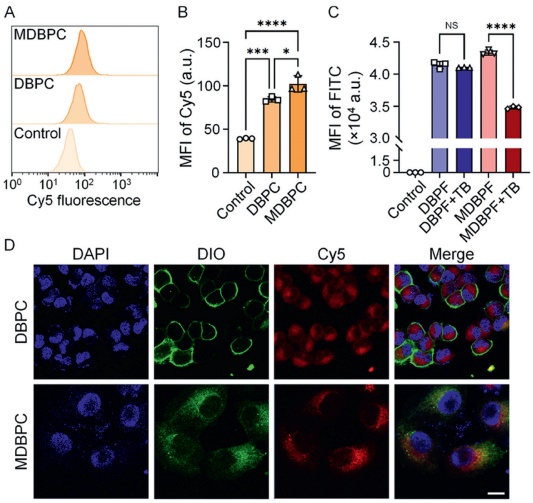

Fig. 3. Attachment of PEGylated-DBCO onto N_3-labeled cytomembrane. (A) Representative Cy5 histograms and (B) quantified MFI values of 143B cells incubated with 50.0 μmol/L Ac_4ManNAz or PBS for 3 days and then stained with DBPC. (C) MFI of 143B cells incubated sequentially with Ac_4ManNAz or PBS and then DBPF, with or without trypan blue treatment. (D) CLSM images of Ac_4ManNAz- or PBS-pretreated 143B cells incubated with DBPC. Cell nuclei and membranes were stained with DAPI and DIO, respectively. Scale bar: 20 μm. Statistical data are represented as mean ± SD ($n = 3$). $^{*}P < 0.05$, $^{***}P < 0.001$, $^{****}P < 0.0001$. Student's *t*-test.

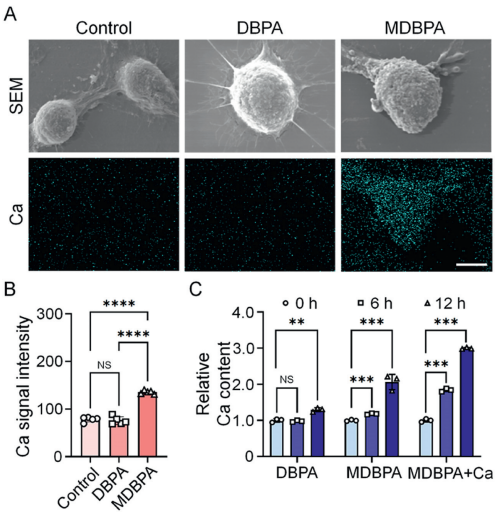

Fig. 4. Biomineralization of 143B cells assisted by metabolic glycoengineering. (A) Representative SEM images and Ca element mapping images of 143B cells incubated sequentially with Ac_4ManNAz or PBS for 3 days and DBPA for 12 h. 143B cells treated with PBS were used as the Control group. Scale bar: 5 μm. (B) Semiquantitative Ca signal intensities calculated from Ca element mapping images. (C) Alterations in relative Ca content of 143B cells with extension of incubation time. Statistical data are represented as mean ± SD ($n = 5$ for B; $n = 3$ for C). $^{**}P < 0.01$, $^{***}P < 0.001$, $^{****}P < 0.0001$. Student's *t*-test.

To assess the reaction activity between PEGylated-DBCO and N_3, DBCO-PEG-Cy5 (DBPC) was synthesized by reacting sulfo-Cy5-amine with DBCO-PEG-NHS. Following the same experimental design as that used for the DBCO-Cy5 labeling, the MFI of 143B cells treated successively with Ac_4ManNAz and DBPC (referred to as MDBPC group) was compared with that of cells without Ac_4ManNAz pretreatment. It turned out that the MFI of MDBPC group was more potent than that of the DBPC group, suggesting that the PEG grafting did not adversely affect the "click chemistry" between DBCO and N_3 (Figs. 3A and B).

Furthermore, DBPA needed to adhere to the cytomembrane to facilitate biomineralization rather than being internalized by tumor cells. To differentiate between intracellular and surface-bound polymers, DBCO-PEG-FITC (DBPF) was synthesized. The localization of polymer was determined using trypan blue, which quenches FITC fluorescence exclusively in the extracellular compartment. As shown in Fig. 3C, there were no apparent differences in MFI before and after the trypan blue treatment of cells incubated with DBPF. By contrast, the MFI of cells in the MDBPF group incubated sequentially with Ac_4ManNAz and DBPF decreased by 19.7% after trypan blue quenching. Moreover, CLSM images illustrated the partial co-localization of cytomembrane (green fluorescence) and DBPC (red fluorescence) in the MDBPC group, whereas approximately all the DBPC was endocytosed by 143B cells after 30-min incubation without Ac_4ManNAz pretreatment (Fig. 3D).

Following their anchorage to the cell membrane, the bisphosphonate groups of DBPA effectively chelated positive ions (predominantly Ca^{2+}), which then facilitated the attraction of negative ions (primarily phosphate (PO_4^{3-})) from the surrounding microenvironments. Scanning electron microscopy (SEM) equipped with an energy dispersive spectrometer (EDS) was used to visualize the pattern of Ca^{2+} deposition on the cytomembrane. As illustrated in Fig. 4A and Fig. S2 (Supporting information), the 143B cells in the MDBPA group (treated sequentially with Ac_4ManNAz for 3 days and with DBPA for 12 h) displayed a prominent Ca signal in the element mapping images. By contrast, a minimal Ca signal was observed on the cell surfaces in the control and DBPA groups. Semiquantitative analysis of the Ca mapping images further underscored the effectiveness of glycometabolism-assisted biomineralization, as detailed in Fig. 4B.

Additionally, inductively coupled plasma mass spectrometry was conducted to quantify the cellular Ca content following various treatments (Fig. 4C). Consistent with the EDS findings, there was a significant increase in Ca content of 143B cells in the MDBPA group. However, cells in the DBPA group exhibited only a slight increase in Ca content, emphasizing the critical role of metabolic pre-conditioning in enhancing biomineralization. Moreover, the extent of ion deposition was found to be dependent on the concentration of Ca^{2+} available in the medium. Specifically, the Ca content of 143B cells in the MDBPA+Ca group that had been pretreated with Ac_4ManNAz for 3 days and then incubated for 12 h in a medium containing DBPA and 10.0 mmol/L Ca^{2+} was about three times higher than that of the Control group, compared with increases of 2.1-fold in the MDBPA group and only 1.3-fold in the DBPA group. These data confirm the influence of Ca^{2+} concentration on the effectiveness of biomineralization, demonstrating that higher levels of available Ca^{2+} significantly enhance biomineralization.

Biomineralization significantly impaired tumor cell viability, migration, and invasion. To evaluate the cytotoxicity of biomineralization, three experimental groups were established, namely, the DBPA, MDBPA, and MDBPA+Ca groups (Fig. 5A). For comparative analysis, 143B cells were also treated with phosphate-buffered saline (PBS; Control group), 10 mmol/L Ca^{2+} (Ca group), or 50.0 μmol/L Ac_4ManNAz. The results indicated that neither a high Ca^{2+} concentration in the microenvironments nor Ac_4ManNAz supplementation adversely affected tumor cell viability relative to the Control group. As expected, the MDBPA and MDBPA+Ca groups exhibited higher cytotoxicity compared to the DBPA group, which could be attributed to the Ca deposition on the cell surface facilitated by "click chemistry". Notably, there was a marked reduction in cell viability in the MDBPA+Ca group, with a 67.4% decrease compared with the Control group; this was substantially higher than the reductions observed in the DBPA (29.1%) and MDBPA (44.3%) groups.

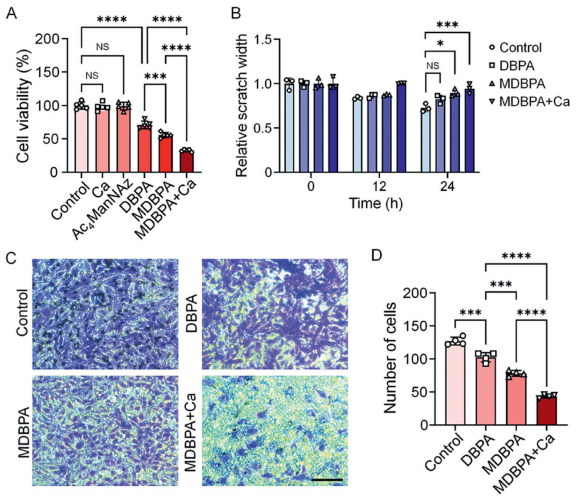

Fig. 5. Biomineralization hampered the viability and mobility of 143B cells. (A) Cell viability of 143B cell after 48 h of Ca deposition induced by DBPA. (B) Relative scratch widths after 0, 12, and 24 h. (C) Representative images taken at bottom of chamber membrane and (D) numbers of invasive cells after 24 h of culture. Scale bar: 100 μm. Statistical data are represented as the mean ± SD ($n = 5$ for A; $n = 3$ for B; $n = 4$ for D). $^{*}P < 0.05$, $^{***}P < 0.001$, $^{****}P < 0.0001$. Student's *t*-test.

Cell mobility is a critical characteristic of tumor malignancy [23]. Here, a scratch assay was employed to assess the impact of biomineralization on tumor cell migratory capabilities (Fig. 5B and Fig. S3 in Supporting information). The scratch width decreased by 27.2% after 24 h in the Control group, whereas the decrease in scratch width was less pronounced in the treatment groups (17.5% in the DBPA group, 10.4% in the MDBPA group, and only 5.7% in the MDBPA+Ca group). This gradient reduction in scratch width across the groups illustrated the effectiveness of biomineralization in curbing cell migration. Moreover, transwell assays showed weakened cell invasiveness after biomineralization, confirming that metabolic glycan labeling significantly mediated Ca deposition (Figs. 5C and D). Specifically, only 61.6% of cells in the MDBPA group traversed the Matrigel to reach the bottom of membrane after 24-h incubation compared with the Control group. Furthermore, the number of invasive cells decreased to 34.3% with an extra 10.0 mmol/L Ca^{2+} addition in the MDBPA+Ca group. By contrast, DBPA treatment moderately affected cell invasion capability, resulting in an invasion rate of 80.7%. These findings suggest that the biomineralization of tumor cells, particularly when intensified by a higher concentration of Ca^{2+}, significantly reduced their mobility, thereby contributing to the therapeutic efficacy of the tumor blockade strategy.

In conclusion, we have successfully developed a tumor-targeting biomineralization strategy facilitated by metabolic glycoengineering. By incorporating the N_3 into tumor cells, the facilely synthesized DBPA was efficiently anchored to the cytomembrane. The attached bisphosphonate groups on the cell surface efficiently attracted positive ions (primarily Ca^{2+}) and negative ions (primarily PO_4^{3-}). Over time, a biomineralized barrier formed around tumor cells, significantly impeding their viability and mobility. Thus, leveraging metabolic glycoengineering-assistant biomineralization, this approach emerges as a promising strategy for *in vivo* tumor suppression.

Declaration of competing interests

The authors declare that they have no known competing financial interests or personal relationships that could have appeared to influence the work reported in this paper.

CRediT authorship contribution statement

Yang Liu: Conceptualization, Validation, Formal analysis, Investigation, Writing – original draft. **Minglu Li:** Conceptualization, Investigation, Writing – review & editing. **Jianxun Ding:** Conceptualization, Writing – review & editing, Supervision, Project administration, Funding acquisition. **Xuesi Chen:** Conceptualization, Writing – review & editing, Supervision, Project administration, Funding acquisition.

Acknowledgments

This work was financially supported by the National Natural Science Foundation of China (Nos. U23A20591 and 52273158) and the Science and Technology Development Program of Jilin Province (Nos. 20240101002JJ and 20210504001GH).

Supplementary materials

Supplementary material associated with this article can be found, in the online version, at doi:10.1016/j.cclet.2024.110146.

References

[1] J. Ding, X. Feng, Z. Jiang, et al., Biomacromolecules 20 (2019) 4258–4271.
[2] D. Zhao, X. Huang, Z. Zhang, et al., Wiley Interdiscip. Rev. Nanomed. Nanobiotechnol. 13 (2021) e1691.
[3] Z. Jiang, Y. Liu, R. Shi, et al., Adv. Mater. 34 (2022) 2110094.
[4] H.F. Dvorak, Cancer J. 21 (2015) 237–243.
[5] D.W. Siemann, Cancer Treat. Rev. 37 (2011) 63–74.
[6] S. Yang, Z. Tang, C. Hu, et al., Adv. Mater. 31 (2019) 1805955.
[7] X.X. Hu, P.P. He, G.B. Qi, et al., ACS Nano 11 (2017) 4086–4096.
[8] D.W. Zheng, S. Hong, Q.L. Zhang, et al., Nat. Commun. 11 (2020) 4907.
[9] Y. Wu, X. Pan, H. Xie, L. Que, X. Tang, Front. Pharmacol. 14 (2023) 1335019.
[10] X. Yang, S. Gao, B. Yang, et al., Adv. Sci. 10 (2023) 2302272.
[11] N. Tang, H. Li, L. Zhang, et al., Angew. Chem. Int. Ed. 60 (2021) 6509–6517.
[12] R. Zhao, B. Wang, X. Yang, et al., Angew. Chem. Int. Ed. 55 (2016) 5225–5229.
[13] Y. Omidi, J. Barar, Bioimpacts 4 (2014) 55–67.
[14] Y. Liu, Z. Jiang, S. Tong, et al., Adv. Mater. 35 (2023) 2203291.
[15] Y. Liu, Y. Zhuang, J. Ding, J. Funct. Polym. 36 (2023) 1–5.
[16] Y. Liu, D. Li, J. Ding, X. Chen, Chin. Chem. Lett. 31 (2020) 3001–3014.
[17] P. Zheng, Y. Liu, J. Chen, et al., Chin. Chem. Lett. 31 (2020) 1178–1182.
[18] J.M. Baskin, C.R. Bertozzi, QSAR Comb. Sci. 26 (2007) 1211–1219.
[19] Y. Ma, S. Yan, X. Xu, H. Cao, R. Wang, Chin. Chem. Lett. 35 (2024) 108645.
[20] H. Wang, R. Wang, K. Cai, et al., Nat. Chem. Biol. 13 (2017) 415–424.
[21] H. Wang, D.J. Mooney, Nat. Chem. 12 (2020) 1102–1114.
[22] H. Lin, H. Hong, L. Feng, et al., Chin. Chem. Lett. 32 (2021) 4041–4044.
[23] M.D. Ryser, B.H. Min, K.D. Siegmund, D. Shibata, Proc. Natl. Acad. Sci. U. S. A. 115 (2018) 5774–5779.